The Trajectory of Dispersed Bubbles around a Taylor Bubble Nose

Boonchai Lertnuwat
Dept. of Mechanical Engineering, Faculty of Engineering,
Chulalongkorn University, Phayathai Rd., Pathum Wan, Bangkok 10330, Thailand

Abstract

Dispersed bubbles in a liquid slug are investigated by theoretical and computational methods. The size of a dispersed bubble is varied to gain the knowledge how it affects the trajectory of the dispersed bubble in the region around the Taylor bubble nose. Considering the translational velocity of the dispersed bubble, the results show that a small dispersed bubble tends to penetrate into a Taylor bubble, whereas a large dispersed bubble tends to turn away from a Taylor bubble. Theoretical analysis explains that the phenomenon is mainly controlled by the terminal velocity of the dispersed bubble, which is high in the case of a small dispersed bubble.

Keywords: Multiphase flow, Slug flow, Dispersed bubble and Translational velocity

1. Nomenclatures

1.1 Characters

a	Radius of sphere
D	Pipe diameter
f	Volumetric fraction
g	Gravity acceleration
i	Coordinates index (z, r, θ)
k	Turbulent kinetic energy
n	Bubble number per unit volume
P	Static pressure
R	Radius in spherical coordinates
r	Radius in cylindrical coordinates
S	Surface
t	Time
V	Total velocity, $\left\|u_z\hat{i}_z + u_r\hat{i}_r + u_\theta\hat{i}_\theta\right\|$
z	Vertical distance in cylindrical coordinates

1.2 Symbols

β	Added mass coefficient
ε	Dissipation
μ	Viscosity
Ω	Volume
θ	Angle in spherical coordinates
ρ	Density

1.3 Superscripts and Subscripts

0	Initial
B	Bubble
d	Drift
e	Effective
G	Gas-phase (or Bubble)
L	Liquid-phase
start	Start position
stop	Stop position
ter	Terminal

2. Introduction

Pipelines in engineering applications usually contain gas-liquid mixtures. Under proper conditions, slug flow occurs. Typically, slug flow is known as a succession of liquid slugs separated by elongation bubbles (Taylor bubbles). For simplicity, slug flow is often studied by being divided into a unit. One unit of slug flow consists of 3 important constituents, i.e. one Taylor bubble, a falling film and a liquid slug. Although the Taylor bubble seems like the only bubble obviously noticeable in a slug unit, there are, as well, many dispersed bubbles suspended in a liquid slug. The dispersed bubbles affect the characteristic of slug flow, for instance if the speed of dispersed bubbles is slower than the speed of the Taylor bubble, they will be merged into the Taylor bubble, resulting in the expansion of the Taylor bubble.

Even though the existence of dispersed bubbles is important, most computational research considers slug flow as a purified liquid without dispersed bubbles {e.g. Mao and Dukler [12]}. A few works consider also the influence of dispersed bubbles by considering them as a

void fraction in a liquid slug without regard to their dimension {e.g. Bugg *et al.* [2] and Clarke and Issa [4]}. In this work, dispersed bubbles are seriously investigated. The computational algorithm, employed in this work, considers both size and translational velocity of dispersed bubbles, so that the pathline of such bubbles will be clearly demonstrated. The radius of a dispersed bubble (R_G) will be varied to see how it affects the trajectory of the dispersed bubble, especially in the region in front of a Taylor bubble, where a liquid-phase flow field develops due to the presence of the Taylor bubble.

3. Computational Algorithm

The algorithm used in this work consists of 9 equations and is shown below:

$$\frac{\partial}{\partial t}\int_{\Omega}\rho_L f_L d\Omega + \int_S \rho_L f_L \vec{V}_L \cdot \hat{n} dS = 0 \qquad (4.1)$$

$$\begin{aligned} f_L &= 1 - f_G \\ &= 1 - \frac{4}{3}\pi R_G^3 n_G \end{aligned} \qquad (4.2)$$

$$\begin{aligned} &\frac{\partial}{\partial t}\int_{\Omega}\rho_L f_L u_{Lz} d\Omega + \int_S \rho_L f_L u_{Lz}\vec{V}_L \cdot \hat{n} dS \\ &= -\int_S P_L \hat{i}_z \cdot \hat{n} dS + \int_S \left(\tau_{zz}\hat{i}_z + \tau_{zr}\hat{i}_r\right)\cdot \hat{n} dS \\ &\quad + \int_{\Omega}\rho_L f_L g_z d\Omega \end{aligned} \qquad (4.3)$$

$$\begin{aligned} &\frac{\partial}{\partial t}\int_{\Omega}\rho_L f_L u_{Lr} d\Omega + \int_S \rho_L f_L u_{Lr}\vec{V} \cdot \hat{n} dS \\ &= -\int_S P_L \hat{i}_r \cdot \hat{n} dS + \int_S \left(\tau_{rz}\hat{i}_z + \tau_{rr}\hat{i}_r\right)\cdot \hat{n} dS \\ &\quad + \int_{\Omega}\rho_L f_L g_r d\Omega + \int_{\Omega}\frac{\tau_{\theta\theta}}{r} d\Omega \end{aligned} \qquad (4.4)$$

$$\begin{aligned} &\frac{d}{dt}\int_{\Omega}\rho k d\Omega + \int_S \rho k \vec{V} \cdot \hat{n} dS \\ &= \int_S \left(\mu + \frac{\mu_t}{\sigma_k}\right)\nabla k \cdot \hat{n} dS + \int_{\Omega} P_k d\Omega \\ &\quad - \int_{\Omega}\rho\varepsilon d\Omega \end{aligned} \qquad (4.5)$$

$$\begin{aligned} &\frac{d}{dt}\int_{\Omega}\rho\varepsilon d\Omega + \int_S \rho\varepsilon \vec{V} \cdot \hat{n} dS \\ &= \int_S \left(\frac{\mu_t}{\sigma_\varepsilon}\right)\nabla\varepsilon \cdot \hat{n} dS + C_{\varepsilon 1}\int_{\Omega} P_k \frac{\varepsilon}{k} d\Omega \\ &\quad - \int_{\Omega}\rho C_{\varepsilon 2}\frac{\varepsilon^2}{k} d\Omega \end{aligned} \qquad (4.6)$$

where

$$\tau_{zz} = 2\mu\frac{\partial u_z}{\partial z}, \tau_{rr} = 2\mu\frac{\partial u_r}{\partial r}, \tau_{\theta\theta} = -2\mu\frac{u_r}{r},$$

$$\tau_{rz} = \tau_{zr} = \mu\left(\frac{\partial u_z}{\partial r} + \frac{\partial u_r}{\partial z}\right),$$

$$P_k = \mu_t\left(\frac{\partial u_i}{\partial x_j} + \frac{\partial u_j}{\partial x_i}\right)\frac{\partial u_i}{\partial x_j} + 2\mu_t\left(\frac{u_r}{r}\right)^2,$$

$$\mu = \mu_e + \mu_t,\ \mu_t = \rho C_\mu \frac{k^2}{\varepsilon},$$

$$\frac{\mu_e}{\mu_L} = (1 - f_G)^{\left[-2.5(\mu_G + 0.4\mu_t)/(\mu_G + \mu_L)\right]},$$

$$C_\mu = 0.09,\ C_{\varepsilon 1} = 1.44,\ C_{\varepsilon 2} = 1.92,$$

$$\sigma_k = 1.0 \text{ and } \sigma_\varepsilon = 1.3$$

$$\frac{\partial}{\partial t}\int_{\Omega} n_G d\Omega + \int_S n_G \vec{V}_G \cdot \hat{n} dS = 0 \qquad (4.7)$$

$$\begin{aligned} &\left(\beta\rho_L \frac{4}{3}\pi R_G^3\right)\left[\frac{\partial}{\partial t}\int_{\Omega} u_{Gz} d\Omega + \int_S u_{Gz}\vec{V}_G \cdot \hat{n} dS\right] \\ &\quad - \left(\beta\rho_L \frac{4}{3}\pi R_G^3\right)\left[\frac{\partial}{\partial t}\int_{\Omega} u_{Lz} d\Omega + \int_S u_{Lz}\vec{V}_L \cdot \hat{n} dS\right] \\ &\quad = -\int_{\Omega}\left(F_{Pz} + F_{Dz}\right) d\Omega \end{aligned} \qquad (4.8)$$

$$\begin{aligned} &\left(\beta\rho_L \frac{4}{3}\pi R_G^3\right)\left[\frac{\partial}{\partial t}\int_{\Omega} u_{Gr} d\Omega + \int_S u_{Gr}\vec{V}_G \cdot \hat{n} dS\right] \\ &\quad - \left(\beta\rho_L \frac{4}{3}\pi R_G^3\right)\left[\frac{\partial}{\partial t}\int_{\Omega} u_{Lr} d\Omega + \int_S u_{Lr}\vec{V}_L \cdot \hat{n} dS\right] \\ &\quad = -\int_{\Omega}\left(F_{\mathrm{Pr}} + F_{Dr}\right) d\Omega \end{aligned} \qquad (4.9)$$

where

$$F_{Pi} = -\frac{4}{3}\pi R_G^3\left(-\nabla_i P_L + \mu_L \nabla^2 u_{Li}\right)$$

$$F_{Di} = \frac{1}{2}\pi R_G^2 \rho_L C_D \left|\vec{V}_G - \vec{V}_L\right|\left(u_{Gi} - u_{Li}\right)$$

$$C_D = \begin{cases} \dfrac{24}{\mathrm{Re}_B}\left(1 + 0.15\,\mathrm{Re}_B^{0.687}\right) & \mathrm{Re}_B \le 1000 \\ 0.438 & \mathrm{Re}_B > 1000 \end{cases}$$

$$\mathrm{Re}_B = \frac{2R_G \rho_L \left|\vec{V}_G - \vec{V}_L\right|}{\mu_L}$$

The continuity equation; (4.1), and the momentum equations; (4.3) and (4.4), are adjusted for governing two-phased flow by coefficient f_L, which is calculated by (4.2)

The k-ε equations; (4.5) and (4.6), look similar to the one-phased model. The only adjustment is the use of effective viscosity (μ_e). The dispersed phase can increase viscosity in a flow system as presented in Ishii and Zuber [10].

The equation of bubble population conservation is presented in (4.7). The meaning of the equation is that the number of dispersed bubbles at inflow must be equal to the number at outflow. This implies that there is neither fission nor fusion of the dispersed bubbles in the considered flow.

The last equations are the equations of a bubble translation motion; (4.8) and (4.9), are used for calculating the translational velocity of a dispersed bubble in z and r directions, respectively. According to the equations, the constituents, which affect the motion of a dispersed bubble, are added mass, pressure difference and drag.

4. Computational Setup

The computational domain covers the unit of slug flow as shown with a gray shade in Fig. 5.1. In this work, axis-symmetric cylindrical coordinates are exploited, due to the symmetry around a pipe centerline of flow in a cylindrical pipe.

For slug flows, most of the experiments use pipes, whose diameters range from 20 to 100 mm. In this work, pipe diameter is chosen to be 50 mm so that it is consistent with the size of pipes used in many experiments as shown in Table 5.1. The length of slug and Taylor bubbles are also selected to be consistent with experimental results from previous works as shown in Table 5.1. Most of the experiments revealed that there was a likely equilibrium size for slug length but not for Taylor bubble length. According to the information in Table 5.1, the length of slug and Taylor bubbles are selected to be $15D$ and $5D$, respectively. Although the length of Taylor bubbles is rather short, they are long enough to prevent the effect of outflow, which may affect the flow field around a Taylor bubble nose.

The shape of a Taylor bubble is predicted with the model proposed by Barnea [1]. The advantage of this model is that it considers as well, the influence of pipe wall friction.

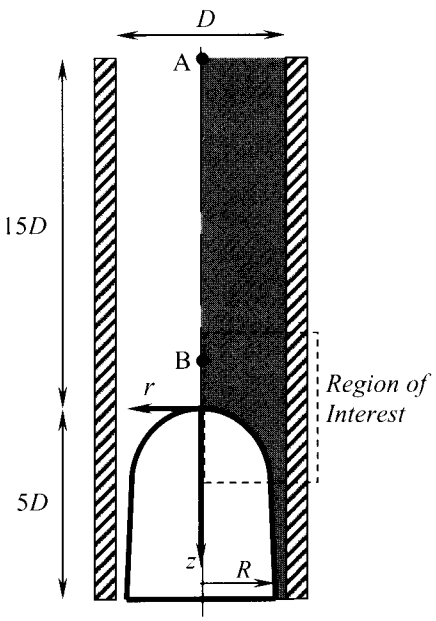

Figure 5.1: The schematic diagram of computation domain, confined to the shaded area.

In simulations, a Taylor bubble is considered as a fixed object, obstructing flow in pipe. Water flows toward a Taylor bubble nose with density of 1000kg/m^3, absolute viscosity of 10^{-3}Ns/m^2 and drift velocity calculated by:

$$u_d = 0.345\sqrt{gD} \qquad (5.1)$$

which is proposed by White and Bearmore [17]. A no-slip condition is posed on the pipe wall. A free-shear boundary condition is posed along the gas-liquid interface since the gas density and viscosity are much less than those of the liquid as explained in Barnea [1]. Along the

centerline of the pipe, a symmetry boundary condition is posed.

On an inlet plane, the velocity is fixed with the value calculated by (5.1). The number of dispersed bubbles is fixed to satisfy the void fraction of 0.26 [see also (4.2)]. This is because Mao and Dukler [11] have found that the void fraction in a liquid slug was 0.26-0.29 and Mi *et al.* [14] have reported that the void fraction was greater than 0.15 in the liquid slug. Referring to Hibiki *et al.* [6], the radius of dispersed bubbles ranges from 0-5.45 mm. Herein, the radius of dispersed bubbles is fixed at two certain sizes, namely 0.1 mm and 0.5 mm, to investigate how the size of dispersed bubble affects the trajectory of the dispersed bubble.

Most of the variables' gradients are set to be zero on the outlet plane, except pressure, which is computed to satisfy the condition of mass conservation and prevent a backward shock wave.

Table 5.1: Statistical Parameters of Gas-Liquid Slug Flow along Vertical Pipes

References	Pipe Dia.	Slug length	Bubble length
Clarke and Issa [4]	50 mm	10-46D	5-23D
Mao and Dukler [13]	50.8 mm		6.2D
Shemer [16]	24 mm	16.3D	
Hout *et al.* [7]	24 mm 54 mm	~17D in 24 mm pipe	4-18.9D in 54 mm pipe
Hout *et al.* [9]	24 mm	16.3D	6.3-28.6D

Flow around Taylor bubbles is predicted by the computational algorithm presented above. The algorithm is discretized by a pressure correction scheme on a finite volume framework. A cylindrical collocated grid system is used. The technique called "Treatment of pressure" is employed to prevent the problem of checkerboard distribution. The no-slip condition along the pipe wall is treated with a wall function, which relies on a logarithmic velocity profile and the equilibrium between production and dissipation of turbulent kinetic energy. The detail of the numerical algorithm can be found in Ferziger and Peric [5].

Grid independence is assured by doubling grids around Taylor a bubble until the discrepancy of mass flowrates across the sectional area at any z is not greater than 1% between coarse and refined grids.

5. Results and Discussion

In this paper, the influence of dispersed bubble size on the trajectory of the dispersed bubbles is investigated. Since the trajectory of dispersed bubbles is investigated in the region around Taylor bubble nose, the results are shown in the region of interest (shown in Figure 5.1).

Figure 6.1 compares liquid-phase velocity fields between 2 cases of different dispersed bubbles, namely the left part belongs to the case that dispersed bubbles have a radius of 0.1 mm and a right part belongs to the case that dispersed bubbles have a radius of 0.5 mm. It shows that the difference between the 2 cases is not significant. This is because the momentum of the gas phase is much smaller than the momentum of the liquid phase. Average void fraction is as much as 0.26.

In contrast, the density distributions between the 2 cases are obviously different. The density is quite uniform in the flow field when R_G equals 0.1 mm, i.e. the density of a gas-liquid mixture becomes as high as the density of the purified liquid just within a narrow space adjacent to the Taylor bubble nose. There is a large space close to Taylor bubble nose where the density of the gas-liquid mixture becomes high when R_G equals 0.5 mm. The buffer region where the density of the mixture is as high as the density of purified liquid reveals that dispersed bubbles cannot flow into this region. This can be explained by gas-phase velocity fields illustrated in Figure 6.2.

Vector plots on the left-hand-side of Figure 6.2 show the velocity field of dispersed bubbles with 0.1 mm R_G. Vector plots on the right-hand-side of the Figure show the gas-phase velocity field in the case that R_G equals 0.5 mm. It is obvious that, along the centerline of pipes, the velocity of smaller dispersed bubbles is faster than that of larger ones. As a result, small dispersed bubbles are more difficult to stop. This can also be proven by theory. Along the centerline of the pipe and at steady state, the velocity of dispersed bubbles can be predicted by integrating (4.8).

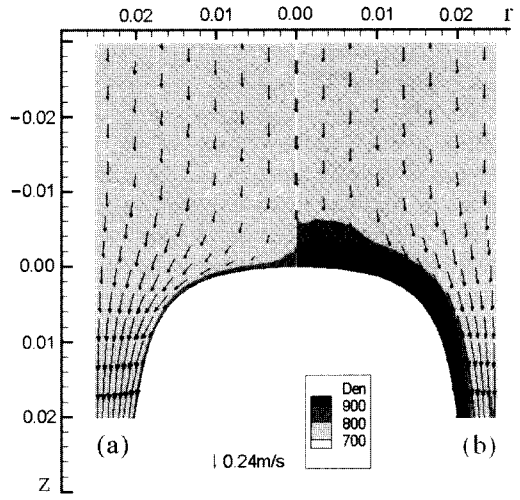

Figure 6.1: Density distribution and liquid-phase velocity field around a Taylor bubble nose (a) R_G =0.1 mm and (b) R_G=0.5 mm *[The vector plots show only every second axial location and every fourth radius location for clarity.]*

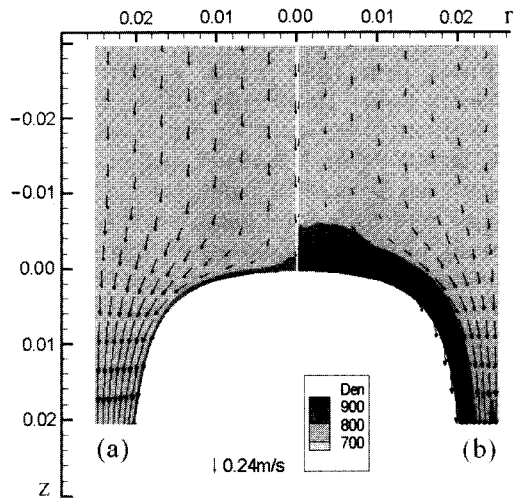

Figure 6.2: Density distribution and gas-phase velocity field around a Taylor bubble nose (a) R_G =0.1 mm and (b) R_G=0.5 mm *[The vector plots show only every second axial location and every fourth radius location for clarity.]*

$$\left(\beta\rho_L\frac{4}{3}\pi R_G^3\right)(2\pi r\cdot\Delta r)\left[\Delta_z u_{Gz}^2-\Delta_z u_{Lz}^2\right]$$
$$=-\frac{4}{3}\pi R_G^3(2\pi r\cdot\Delta r\cdot\Delta z)\frac{\partial P_L}{\partial z}$$
$$-6\pi R_G\mu_L\left[1+0.15\left(\frac{2\rho_L R_G|\overline{u_{Gz}-u_{Lz}}|}{\mu_L}\right)^{0.687}\right]$$
$$(2\pi r\cdot\Delta r\cdot\Delta z)(\overline{u_{Gz}-u_{Lz}})$$

$$\left(\beta\rho_L R_G^2\right)\left[\Delta_z u_{Gz}^2-\Delta_z u_{Lz}^2\right]=-R_G^2\frac{\partial P_L}{\partial z}\Delta z$$
$$-\frac{9}{2}\mu_L\left[1+0.15\left(\frac{2\rho_L R_G|\overline{u_{Gz}-u_{Lz}}|}{\mu_L}\right)^{0.687}\right]$$
$$(\overline{u_{Gz}-u_{Lz}})\Delta z \qquad (6.1)$$

If dispersed bubbles approach the Taylor bubble nose with terminal velocity, the magnitude of velocity is calculated by neglecting the left-hand-side of (6.1). Consequently, we obtain:

$$(\overline{u_{Gz}-u_{Lz}})=-\frac{2}{9}\frac{R_G^2}{\mu_L}\frac{\partial P_L}{\partial z}$$
$$\left[1+0.15\left(\frac{2\rho_L R_G|u_{Gz}-u_{Lz}|}{\mu_L}\right)^{0.687}\right]^{-1} \qquad (6.2)$$

If we assume that dispersed bubbles can achieve terminal velocity very far from the Taylor bubble nose (within the region between point A and B in Figure 5.1), liquid-phase velocity will equal u_d and pressure gradient will equal $\rho_L g$. This changes (6.2) to be:

$$u_{Gz,ter}=u_d-\frac{2}{9}\frac{R_G^2\rho_L g}{\mu_L}$$
$$\left[1+0.15\left(\frac{2\rho_L R_G|\overline{u_{Gz}-u_{Lz}}|}{\mu_L}\right)^{0.687}\right]^{-1} \qquad (6.3)$$

The equation above implies that the magnitude of u_{Gz} depends on R_G, and it reaches a maximum when R_G is zero.

The consequent question is whether or not dispersed bubbles can achieve terminal velocity

before they reach point B in front of the Taylor bubble nose as the previous assumption. Therefore the distance needed for achieving terminal velocity is to be estimated by re-arranging (6.1) as:

$$\Delta z = -\beta\rho_L\left[\Delta_z u_{Gz}^2 - \Delta_z u_{Lz}^2\right]\left\{\frac{\partial P_L}{\partial z} + \left(\overline{u_{Gz} - u_{Lz}}\right)\right.$$
$$\left.\frac{9}{2}\frac{\mu_L}{R_G^2}\left[1 + 0.15\left(\frac{2\rho_L R_G\left|\overline{u_{Gz} - u_{Lz}}\right|}{\mu_L}\right)^{0.687}\right]\right\}^{-1}$$

Then, substituting pressure gradient with $\rho_L g$, and assuming that the liquid phase is fully developed in a liquid slug. This is true when a liquid slug is long enough.

$$\Delta z_{ter} = -\beta\left[u_{Gz,ter}^2 - u_{Gz,0}^2\right]\left\{g + \left(\overline{u_{Gz} - u_{Lz}}\right)\right.$$
$$\left.\frac{9}{2}\frac{\mu_L}{\rho_L R_G^2}\left[1 + 0.15\left(\frac{2\rho_L R_G\left|\overline{u_{Gz} - u_{Lz}}\right|}{\mu_L}\right)^{0.687}\right]\right\}^{-1} \quad \text{-(6.4)}$$

With (6.2), (6.4) and approximating $\overline{(u_{Gz}-u_{Lz})} = 0.5(u_{Gz,ter}-u_d)$, we will be able to calculate $u_{Gz,ter}$ and Δz_{ter} as shown in Table 6.1.

Table 6.1: Terminal velocity and distance needed to achieve the terminal velocity of dispersed bubbles with different R_G's.

R_G (mm)	$u_{Gz,ter}$ (m/s)	Δz_{ter} (m)	$Re_{B,ter}$
0.1	0.225	$0.73\text{x}10^{-3}$	3.31
0.5	0.128	$3.33\text{x}10^{-3}$	114

Note: Let $u_{Gz,0}=u_d$.

It is clear that dispersed bubbles can achieve terminal velocity since Δz_{ter} is much shorter than the length of a liquid slug (see Table 5.1), consistent with the assumption. In addition, Table 6.1 shows that the terminal velocity of a small dispersed bubble is approximately 2 times larger than that of a large dispersed bubble. This agrees well with the simulation results in Figure 6.2. Faster terminal velocity tends to push a small dispersed bubble to flow toward the Taylor bubble nose before the bubble stops very close to the nose. The distance needed for stopping a dispersed bubble may be predicted. However, before predicting the distance needed for stopping a dispersed bubble along the pipe centerline, it is necessary to estimate the pressure gradient along the pipe centerline in the region close to the Taylor bubble nose. Referring to the work of Mao and Dukler [12], the geometry in the front of a Taylor bubble nose looks like a sphere. The conventional velocity functions for flow around a sphere thus, are exploited.

$$u_{Lz} = -u_d\left(1 - \frac{a^3}{R^3}\cos^2\theta + \frac{a^3}{2R^3}\sin^2\theta\right)$$
$$u_{Lr} = -u_d\left(\frac{3}{2}\frac{a^3}{R^3}\sin\theta\cos\theta\right)$$

in which, R and θ are spherical coordinates as illustrated in Figure 6.3.

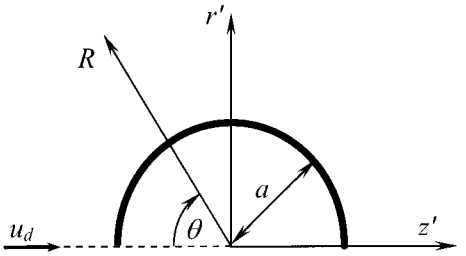

Figure 6.3: Flow around a sphere (radius=a) and the coordinate system.

In the case that we consider only liquid-phase velocity along pipe centerline (θ=0), we obtain:

$$u_{Lz} = -u_d\left(1 - \frac{a^3}{R^3}\right) \quad (6.5)$$

$$u_{Lr} = 0 \quad (6.6)$$

The pressure gradient in the liquid around the sphere can be calculated by using the momentum equation of steady inviscid flow.

$$\int_S \rho_L u_{Lz}\vec{V}_L \cdot \hat{n}dS = -\int_S P_L \hat{i}_z \cdot \hat{n}dS + \int_\Omega \rho_L g_z d\Omega \quad (6.7)$$

Using divergence theorem (6.7), this leads to:

$$\int_\Omega \rho_L \vec{\nabla} \cdot \left(u_{Lz}\vec{V}_L\right)\hat{n}d\Omega$$

$$= -\int_{\Omega} \frac{\partial P_L}{\partial z} d\Omega + \int_{\Omega} \rho_L g_z d\Omega$$

$$\frac{\partial P_L}{\partial z} = \rho_L g - \rho_L \left(\frac{\partial u_{Lz} u_{Lz}}{\partial z} + \frac{\partial u_{Lz} u_{Lr}}{\partial r} \right) \quad (6.8)$$

Since we have known that, along the pipe centerline in front of a Taylor bubble nose, $R^2 = (-z')^2$, the gradients of velocities products in (6.8) can be determined by employing (6.5) and (6.6):

$$\frac{\partial u_{Lz} u_{Lz}}{\partial z} = -6u_d^2 \left(1 + \frac{a^3}{z'^3} \right) \frac{a^3}{z'^4} \quad (6.9)$$

$$\frac{\partial u_{Lz} u_{Lr}}{\partial r} = 0 \quad (6.10)$$

Moving the origin of the coordinate system in Figure 6.3 to the nose of Taylor bubble so that it will be consistent with the coordinate system in Figure 5.1, (6.9) becomes:

$$\frac{\partial u_{Lz} u_{Lz}}{\partial z} = -6u_d^2 \left(1 + \frac{a^3}{(z-a)^3} \right) \frac{a^3}{(z-a)^4} \quad (6.11)$$

Substituting (6.10) and (6.11) into (6.8), we get:

$$\frac{\partial P_L}{\partial z} = \rho_L g + 6\rho_L u_d^2 \left(1 + \frac{a^3}{(z-a)^3} \right) \frac{a^3}{(z-a)^4}$$

Using (5.1) to determine u_d, and approximating that $D \approx 2a$, finally we get:

$$\frac{\partial P_L}{\partial z} \approx \rho_L g \left[1 + 1.4 \left(1 + \frac{a^3}{(z-a)^3} \right) \frac{a^4}{(z-a)^4} \right] \quad \text{-(6.12)}$$

The equation above states that a pressure gradient in a liquid around a sphere is a function of z. The maximum pressure gradient is approximately $1.3\rho_L g$, occurring at z=-0.2a. The second term in parentheses on the right-hand-side of (6.12) decreases to be –0.1 at z=-0.9a (~0.45D) and –0.01 at z=-2.5a (~-1.25D). This agrees well with experimental results, which demonstrate that the influence of the Taylor bubble is detectable in the liquid slug only at a distance closer than 1D from the Taylor bubble nose. {Hout *et al.* [8], Bugg and Saad [3], Polonsky *et al.* [15]}

The distance needed for stopping a dispersed bubble along the pipe centerline is estimated by substituting (6.11) and (6.12) into (6.1).

$$\left(\beta\rho_L R_G^2\right) \left[\Delta_z u_{Gz}^2 + 1.4g \left(1 + \frac{a^3}{(z-a)^3} \right) \frac{a^4}{(z-a)^4} \Delta z \right]$$

$$= -R_G^2 \rho_L g \left[1 + 1.4 \left(1 + \frac{a^3}{(z-a)^3} \right) \frac{a^4}{(z-a)^4} \right] \Delta z$$

$$- \frac{9}{2} \mu_L \left[1 + 0.15 \left(\frac{2\rho_L R_G |\overline{u_{Gz} - u_{Lz}}|}{\mu_L} \right)^{0.687} \right] (\overline{u_{Gz} - u_{Lz}}) \Delta z$$

$$\Delta z_{stop} = -\beta \left(u_{Gz,stop}^2 - u_{Gz,start}^2 \right)$$

$$\left\{ \left[1 + 1.4(1+\beta) \left(1 + \frac{a^3}{(z-a)^3} \right) \frac{a^4}{(z-a)^4} \right] g \right.$$

$$+ \frac{9}{2} \frac{\mu_L}{\rho_L R_G^2} \left[1 + 0.15 \left(\frac{2\rho_L R_G |\overline{u_{Gz} - u_{Lz}}|}{\mu_L} \right)^{0.687} \right]$$

$$\left. (\overline{u_{Gz} - u_{Lz}}) \right\}^{-1}$$

According to Figure 5.1, point B is assumed to be the last point where a dispersed bubble can maintain its velocity to be terminal velocity, before the velocity of the dispersed bubble starts to develop, due to the presence of the Taylor bubble. This probably assumes that point B is located on the position where z = -2.5a, since the influence of Taylor bubble on a pressure gradient is only 1% of the gravity effect as predicted by (6.12). Assuming that at z=-2.5a, $u_{Gz,start}^2 = u_{Gz,ter}^2$.

$$\Delta z_{stop} = -\beta \left(0 - u_{Gz,ter}^2 \right)$$

$$\left\{ \left[1 + 1.4(1+\beta) \left(1 + \frac{1}{(-3.5)^3} \right) \frac{a^4}{(-3.5)^4} \right] g \right.$$

$$+ \frac{9}{2} \frac{\mu_L}{\rho_L R_G^2} \left[1 + 0.15 \left(\frac{2\rho_L R_G |\overline{u_{Gz} - u_{Lz}}|}{\mu_L} \right)^{0.687} \right]$$

$$\left. (\overline{u_{Gz} - u_{Lz}}) \right\}^{-1}$$

$$\Delta z_{stop} = \beta u_{Gz,ter}^2 \left\{1.014g + \frac{9}{2}\frac{\mu_L}{\rho_L R_G^2}\left[1+0.15\left(\frac{2\rho_L R_G|\overline{u_{Gz}-u_{Lz}}|}{\mu_L}\right)^{0.687}\right](\overline{u_{Gz}-u_{Lz}})\right\}^{-1} \quad (6.13)$$

Substituting $u_{Gz,ter}$, R_G from Table 6.1 and assuming that $(\overline{u_{Gz}-u_{Lz}}) = 0.5(u_{Gz,ter}-u_d)$, (6.13) gives:

Δz_{stop} = 4.66 mm for R_G = 0.1 mm, and
Δz_{stop} = 1.26 mm for R_G = 0.5 mm.

That is, the discrepancy between the 2 cases is 3.4 mm, while the simulation results in Figure 6.2 shows that the discrepancy of Δz_{stop} between the 2 cases is approximately 4 mm. Hence (6.13) underestimates Δz_{stop}, but still gives results in the same order of magnitude. The equation shows that the distance Δz_{stop} mainly varies with $u_{Gz,ter}$, which is high for small dispersed bubbles, resulting in long Δz_{stop}. This explains the reason why small dispersed bubbles can flow closer toward the Taylor bubble nose than large dispersed bubbles.

6. Conclusion

1. Small dispersed bubbles tend to penetrate into Taylor bubbles, whereas large dispersed bubbles tend to turn away from Taylor bubbles.

2. The trajectory of dispersed bubbles leads to a buffer region in front of Taylor bubble noses, where dispersed bubbles cannot penetrate inward.

3. The size of buffer regions is resulted from:

3.1 Terminal velocity of dispersed bubbles,
3.2 Gravitational acceleration,
3.3 The trajectory of liquid phases,
3.4 Drag on dispersed bubbles.

However, the first constituent is the most important for buffer size.

7. References

[1] Barnea, D., Effect of Bubble Shape on Pressure Drop Calculations in Vertical Slug Flow, Int. J. Multiphase Flow, Vol.16 No.1, pp.79-89, 1990.

[2] Bugg, J. D., Mack, K. and Rezkallah, K. S., A Numerical Model of Taylor Bubbles Rising Through Stagnant Liquids in Vertical Tubes, Int. J. Multiphase Flow, Vol. 24, pp. 271-281, 1998.

[3] Bugg, J. D. and Saad, G. A., The Velocity Field around a Taylor Bubble Rising in a Stagnant Viscous Fluid: Numerical and Experimental Results, Int. J. Multiphase Flow, Vol. 28, pp. 791-803, 2002.

[4] Clarke, A. and Issa, R. I., A Numerical Model of Slug Flow in Vertical Tubes, Computers & Fluids, Vol. 26, No. 4, pp. 395-415, 1997.

[5] Ferziger, J. H. and Peric, M., Computational Methods for Fluid Dynamics, 3rd ed., Springer-Verlag, Germany, pp. 157-308, 2002.

[6] Hikibi, T., Goda, H. Kim, S. Ishii, M., and Uhle, J., Structure of Vertical Downward Bubbly Flow, International Journal of Heat and Mass Transfer, Vol. 47, pp. 1847-1862, 2004.

[7] Hout, R. V., Bernea, D., and Shemer, L., Evolution of Statistical Parameters of Gas-Liquid Slug Flow along Vertical Pipes, Int. J. Multiphase Flow, Vol. 27, pp. 1579-1602, 2001.

[8] Hout, R. V., Gulitski, A., Barnea, D. and Shemer, L., Experimental Investigation of the Velocity Field Induced by a Taylor Bubble Rising in Stagnant Water, Int. J. Multiphase Flow, Vol. 28, pp. 579-596, 2002.

[9] Hout, R. V., Bernea, D., and Shemer, L., Evolution of Hydrodynamic and Statistical Parameters of Gas-Liquid Slug Flow along Inclined Pipes, Chemical Engineering Science, Vol. 58, pp. 115 – 133, 2003.

[10] Ishii, M., and Zuber, N., Drag Coefficient and Relative Velocity in Bubbly, Droplet or Particulate Flows, AIChE Journal, Vol. 25 No. 5, pp.843-855, September 1979

[11] Mao, Z-S. and Dukler, A. E., Rise Velocity of a Taylor Bubble in a Train of Such Bubbles in a Flowing Liquid, Chemical Engineering Science, Vol. 40 No. 11, pp. 2158-2160, 1985.

[12] Mao, Z-S. and Dukler, A. E., The Motion of Taylor Bubbles in Vertical Tubes I. A Numerical Simulation for the Shape and Rise Velocity of Taylor Bubbles in Stagnant and Flowing Liquid, Journal of Computational Physics, Vol. 91, pp. 132-160, 1990.

[13] Mao, Z-S. and Dukler, A. E. , The Motion of Taylor Bubbles in Vertical Tubes-II. Experimental Data and Simulations for Laminar and Turbulent Flow, Chemical Engineering Science, Vol. 46, No. 8, pp. 2055-2064, 1991.

[14] Mi, Y., Ishii, M. and Tsoukalas, L. H., Investigation of Vertical Slug Flow with Advanced Two-Phase Flow Instrumentation, Nuclear Engineering and Design, Vol. 204, pp. 69-85, 2001.

[15] Polonsky, S., Shemer, L. and Barnea, D., The Reletion Between the Taylor Bubble Motion and the Velocity Field Ahead of It, Int. J. Multiphase Flow, Vol. 25, pp. 957-975, 1999.

[16] Shemer, V., Hydrodynamic and Statistical Parameters of Slug Flow, International Journal of Heat and Fluid Flow, Vol. 24, pp. 334–344, 2003.

[17] White, E. T. and Beardmore, R. H., The Velocity of Rise of Single Cylindrical Air Bubbles through Liquids Contained in Vertical Tubes, Chemical Engineering Science, Vol. 17, pp. 351-361, 1962.